Sensorless Direct Field-Oriented Control of Three-Phase Induction Motor Drives for Low-Cost Applications

(Article begins on next page)

28 April 2024

Sensorless Direct Field-Oriented Control of Three-Phase Induction Motor Drives for Low-Cost Applications

Radu Bojoi, *Member, IEEE*, Paolo Guglielmi, *Member, IEEE*, and Gian-Mario Pellegrino, *Member, IEEE*

Abstract—A sensorless direct rotor field-oriented control (SDRFOC) scheme of three-phase induction motors for low-cost applications is presented in this paper. The SDRFOC algorithm is based on a sensorless closed-loop rotor flux observer whose main advantages are simplicity and robustness to motor parameter detuning. The whole algorithm has been developed and implemented on a low-cost fixed-point digital signal processor controller. Experimental results are presented for a 0.5-kW induction motor drive for a primary vacuum pump used in industry applications.

Index Terms—Digital control, digital signal processor (DSP), induction motor drive, low-cost applications, sensorless field-oriented control (SFOC).

I. INTRODUCTION

CONTROLLED induction motor drives without mechanical speed sensors have the advantage of reduced cost and high reliability. Low-power low-cost applications usually adopt V/Hz scalar control when no particular dynamic performance is required. Variable-speed pumps, fans, and appliances can be mentioned as examples. Furthermore, these applications usually do not require zero-speed operation and often do not need accurate speed estimation. The main advantage of V/Hz control is its simplicity and for this reason it has been traditionally implemented using low-cost microcontrollers.

During the last few years, a particular interest has been noted on applying sensorless field-oriented control (SFOC) to the aforementioned applications. The continuous development of digital signal processors (DSPs), together with the reduction of power electronics cost, has allowed the use of DSPs that are able to implement advanced control algorithms, such as SFOC [1].

The key issue for an SFOC is how to obtain an accurate machine flux estimate to get a decoupled control of the machine flux and torque. In addition, the rotor speed estimation is also needed for speed control. Although many research efforts have been dedicated to propose simple and robust SFOC algorithms

as alternatives to the existing V/Hz control schemes, the SFOC schemes cannot be yet considered as standards for low cost applications.

In the last two decades, intensive research work has been dedicated to SFOC schemes for induction machines and many different algorithms for the machine flux estimation using only electrical quantities (voltages and currents) have been proposed. These algorithms can be divided into two main groups [2]: 1) closed-loop observers and 2) open-loop estimators. The closed-loop observers use an internal feedback loop together with the machine model to improve the flux estimation accuracy and robustness against parameter variations. For this reason, they are preferred for industrial applications. The open-loop estimators are based only on the machine model and exhibit lower performance compared with the closed-loop observers in terms of accuracy.

Various control schemes dealing with closed-loop observers have been reported in the literature. The model reference adaptive system approach [3] is based on the comparison between the outputs of two machine models: the first one (reference model) does not contain the rotor speed, while the second one (adaptive model) uses the speed to estimate the machine flux. The outputs of the two models are compared to obtain an error signal. The error is the input of a proper adaptation mechanism to generate the estimated speed which is fed back to the adaptive model. This solution requires open-loop integration and drift problems could appear; this aspect is solved using a low-pass filter (LPF) instead of an integrator.

The adaptive-observers (AO) approach, using the Luenberger [4] observer or the Kalman filter [5], gets accurate flux and speed estimates under detuned operating conditions. The key issue of the AO is the computation of their gain matrix to get stability and optimum filtering when both inputs and outputs are corrupted by noise (Kalman filter). These solutions are still considered computationally intensive or difficult to tune, so their application in low cost drives is limited.

The sliding-mode observers [6]–[10] are considered as a promising control solution for industry applications due to their robustness against parameter detuning and their reduced order compared to the Luenberger observer and Kalman filter.

The goal of this paper is to propose a simple and robust sensorless direct rotor field-oriented control (SDRFOC) scheme for low cost applications to replace the existing V/Hz control schemes. Such an SDRFOC improves the motor exploitation (torque, power factor) and the drive efficiency. The proposed

scheme is based on a sensorless closed-loop rotor flux observer. This algorithm is very effective for low cost applications where accuracy in the speed estimation is not mandatory. The SDRFOC scheme has been developed and implemented on a low-cost fixed-point DSP-based controller. Experimental results are presented for a 0.5-kW induction motor drive for a primary vacuum pump used in industry applications.

II. ROTOR FLUX OBSERVER

A. Machine Model

The machine dynamic model is obtained using normalized quantities. The base quantities for normalization are given in the Appendix. The normalization procedure is necessary for digital implementation using fixed-point processors. It has been found that it is convenient to normalize the machine model using the full-scale values of the current/voltage acquisition and the maximum value of the electrical speed. The dynamic normalized voltage and flux equations in stationary reference frame are given in (1) under the common assumptions of sinusoidal winding distributions, magnetic linearity and no iron losses

$$\begin{cases} \bar{v}_{\rm s} = r_{\rm s} \cdot \bar{i}_{\rm s} + \dfrac{1}{\omega_{\rm base}} \cdot \dfrac{d}{dt}\bar{\lambda}_{\rm s} \\ 0 = r_{\rm r} \cdot \bar{i}_{\rm r} + \dfrac{1}{\omega_{\rm base}} \cdot \dfrac{d}{dt}\bar{\lambda}_{\rm r} - j \cdot \omega_{\rm r} \cdot \bar{\lambda}_{\rm r} \end{cases}$$

$$\begin{cases} \bar{\lambda}_{\rm s} = l_{\rm s} \cdot \bar{i}_{\rm s} + l_{\rm m} \cdot \bar{i}_{\rm r} \\ \bar{\lambda}_{\rm r} = l_{\rm m} \cdot \bar{i}_{\rm s} + l_{\rm r} \cdot \bar{i}_{\rm r}. \end{cases} \quad (1)$$

By eliminating the rotor current using the flux equations, the machine voltage equations become

$$\begin{cases} \dfrac{1}{\omega_{\rm base}} \cdot \dfrac{d}{dt}\bar{\lambda}_{\rm s} = -r_{\rm s} \cdot \bar{i}_{\rm s} + \bar{v}_{\rm s} \\ \dfrac{1}{\omega_{\rm base}} \cdot \dfrac{d}{dt}\bar{\lambda}_{\rm r} = \dfrac{l_{\rm m}}{\tau_{\rm rn}} \cdot \bar{i}_{\rm s} + \left(-\dfrac{1}{\tau_{\rm rn}} + j \cdot \omega_{\rm r}\right)\bar{\lambda}_{\rm r} \end{cases} \quad (2)$$

where $\tau_{\rm rn} = l_{\rm r}/r_{\rm r}$ is the normalized rotor time constant.

B. Sensorless Rotor Flux Observer

The stator voltage equations (or the stator model) can be used to estimate the rotor flux components in stationary (α, β) reference frame without information on the rotor speed. This solution, known as the voltage–current $(V{-}I)$ estimator, first estimates the stator flux vector by voltage integration; the rotor flux vector is obtained as

$$\hat{\bar{\lambda}}_{\rm r} = k_{\rm r}^{-1} \cdot (\hat{\bar{\lambda}}_{\rm s} - \sigma \cdot l_{\rm s} \cdot \bar{i}_{\rm s}) \quad (3)$$

where $\hat{\bar{\lambda}}_{\rm s} = \omega_{\rm base} \cdot \int (\bar{v}_{\rm s} - r_{\rm s} \cdot \bar{i}_{\rm s})dt$, σ is the total leakage factor and $k_{\rm r} = l_{\rm m}/l_{\rm r}$.

The flux estimator based on the stator model is simple but requires open-loop integration with drift problems for real implementations. For this reason, an LPF is usually adopted instead of a pure integrator [11]. This solution requires a phase compensation scheme for low speed operation and is very sensitive to stator resistance variation.

The proposed rotor flux observer is based on the $V{-}I$ estimator in a closed-loop scheme without any LPF. The internal
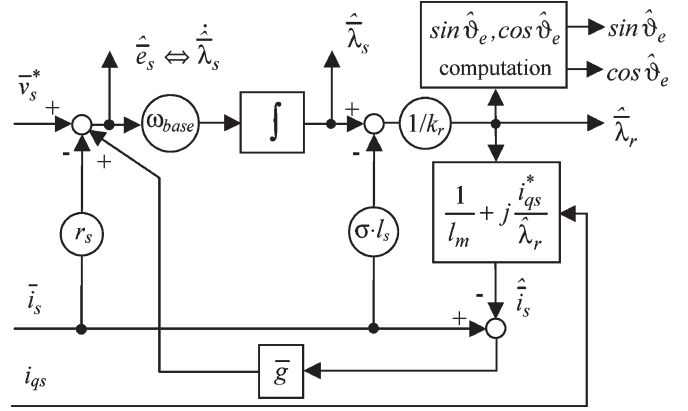

Fig. 1. Sensorless rotor flux observer.

feedback is obtained by manipulating the rotor model. Thus, the rotor flux derivative is approximated in (2) with its steady-state expression

$$\frac{1}{\omega_{\rm base}} \cdot \frac{d}{dt}\bar{\lambda}_{\rm r} \cong j \cdot \omega_{\rm e} \cdot \bar{\lambda}_{\rm r} \quad (4)$$

where $\omega_{\rm e}$ is the normalized electrical speed.

In this case, from (2) and (4), the stator current vector can be obtained from the rotor flux [12] as

$$\hat{\bar{i}}_{\rm s} = \left(\frac{1}{l_{\rm m}} + j \cdot \frac{\omega_{\rm slip} \cdot \tau_{\rm rn}}{l_{\rm m}}\right) \cdot \hat{\bar{\lambda}}_{\rm r}, \qquad \omega_{\rm slip} = \omega_{\rm e} - \omega_{\rm r}. \quad (5)$$

The slip speed $\omega_{\rm slip}$ is computed in the (d, q) synchronous reference frame aligned with the rotor flux as

$$\omega_{\rm slip} = \frac{l_{\rm m} \cdot i_{qs}}{\tau_{\rm rn} \cdot \hat{\lambda}_{\rm r}} \quad (6)$$

where $\hat{\lambda}_{\rm r} = \sqrt{\hat{\lambda}_{{\rm r}\alpha}^2 + \hat{\lambda}_{{\rm r}\beta}^2}$ is the magnitude of the rotor flux vector and i_{qs} is the q-axis component of the measured stator current vector in (d, q) reference frame.

Combining (5) and (6) yields

$$\hat{\bar{i}}_{\rm s} = \left(\frac{1}{l_{\rm m}} + j \cdot \frac{i_{qs}}{\hat{\lambda}_{\rm r}}\right) \cdot \hat{\bar{\lambda}}_{\rm r}. \quad (7)$$

The estimated stator current components in stationary reference frame will be

$$\begin{cases} \hat{i}_{{\rm s}\alpha} = \frac{1}{l_{\rm m}} \cdot \hat{\lambda}_{{\rm r}\alpha} - i_{qs} \cdot \sin\hat{\vartheta}_{\rm e} \\ \hat{i}_{{\rm s}\beta} = \frac{1}{l_{\rm m}} \cdot \hat{\lambda}_{{\rm r}\beta} + i_{qs} \cdot \cos\hat{\vartheta}_{\rm e} \end{cases} \quad (8)$$

where the sine and cosine functions of the rotor flux vector position are $\sin\hat{\vartheta}_{\rm e} = \hat{\lambda}_{{\rm r}\beta}/\hat{\lambda}_{\rm r}$, $\cos\hat{\vartheta}_{\rm e} = \hat{\lambda}_{{\rm r}\alpha}/\hat{\lambda}_{\rm r}$.

The rotor flux observer presented in this paper is reported in Fig. 1. As already mentioned, the scheme is based on the $V{-}I$ estimator: the internal feedback is provided by the error between the measured and the estimated stator current vectors. The observer is a reduced-order scheme since the observer state variables are only the stator flux components in the (α, β) reference frame.
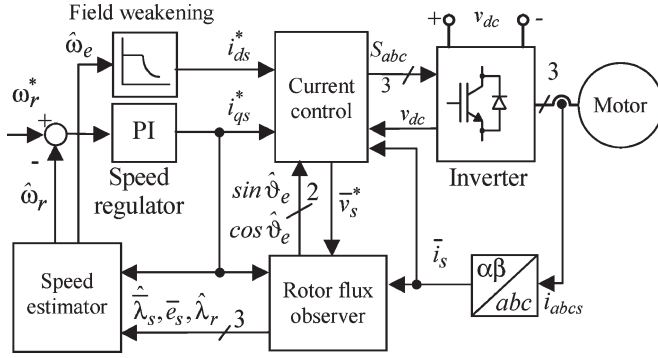
Fig. 2. SDRFOC scheme.

Fig. 3. Dead-time compensation scheme.

The current error is fed back to the observer input through a complex gain $\bar{g} = g_{\mathrm{re}} + j \cdot g_{\mathrm{im}}$. The presence of the imaginary part improves the observer response during transients. As shown by Fig. 1, the rotor flux observer is simple to implement with low-cost fixed-point DSP controllers. The internal feedback gives robustness against motor parameter variations and allows use of a pure integrator for stator flux estimation (avoiding LPFs and related phase compensation schemes).

As usual for rotor field-oriented control (FOC) schemes, the current control imposes the d-axis (flux-producing) and q-axis (torque-producing) stator current components. If the current control scheme is implemented in synchronous reference frame, it is more convenient to use in (8) the reference value of the q-axis current instead of the noisy measured one (Fig. 1). The observer input is the voltage command vector in stationary reference frame.

III. SENSORLESS ROTOR FOC

The rotor flux observer has been tested in an SDRFOC scheme, whose block diagram is shown in Fig. 2. The rotor speed is estimated by means of the electrical speed and the slip speed as

$$\hat{\omega}_{\mathrm{r}} = \hat{\omega}_{\mathrm{e}} - \hat{\omega}_{\mathrm{slip}}. \qquad (9)$$

The slip speed is computed using (6) with the q-axis reference value instead of the measured one to have a smoother speed estimate. The electrical speed (10) is computed by means of the stator flux components and their time derivatives, which are the stator back EMFs $\hat{e}_{\mathrm{s}\alpha}$, $\hat{e}_{\mathrm{s}\beta}$ (see Figs. 1 and 2)

$$\hat{\omega}_{\mathrm{e}} = \frac{\hat{\lambda}_{\mathrm{s}\alpha} \cdot \dot{\hat{\lambda}}_{\mathrm{s}\beta} - \hat{\lambda}_{\mathrm{s}\beta} \cdot \dot{\hat{\lambda}}_{\mathrm{s}\alpha}}{\hat{\lambda}_{\mathrm{s}}^2} = \frac{\hat{\lambda}_{\mathrm{s}\alpha} \cdot \hat{e}_{\mathrm{s}\beta} - \hat{\lambda}_{\mathrm{s}\beta} \cdot \hat{e}_{\mathrm{s}\alpha}}{\hat{\lambda}_{\mathrm{s}}^2} \qquad (10)$$

where $\hat{\lambda}_{\mathrm{s}} = \sqrt{\hat{\lambda}_{\mathrm{s}\alpha}^2 + \hat{\lambda}_{\mathrm{s}\beta}^2}$ is the magnitude of the stator flux vector.

It must be underlined that (10) does not involve time derivative computation when back EMF voltages are used. For this reason, the electrical speed estimate is smoother compared with algorithms using time derivatives of the stator flux [10]. Moreover, this solution is straightforward and simpler compared with other phase-locked-loop-based algorithms.
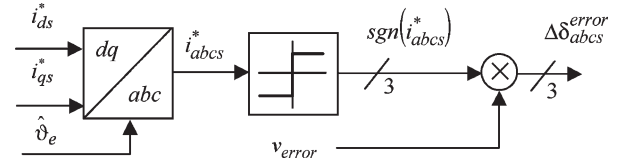
The field orientation is insensitive to rotor resistance detuning. A constant value for l_{m} (in Fig. 1) results in a small orientation error when magnetic saturation occurs. A proper choice of the l_{m} value limits this error to negligible values in the whole operation range. The only sensitive parameter is the stator resistance r_{s}, and only at low speed. A high feedback gain $\bar{g}$ limits the effects of r_{s} detuning on the field orientation, together with the effects of the stator voltage estimation errors. The adaptation of $\bar{g}$ to the actual speed is an option since the effects of r_{s} detuning are no longer important at high speed. The reduction of $\bar{g}$ at high speed improves the observer stability. The imaginary part of the complex gain has similar effects at high speed and nearly no significance at low speed. Refer to Appendix for the complex gain value.

As illustrated in Fig. 1, the flux observer is fed by the stator voltage vector command in stationary reference frame. For the FOC schemes, it is always convenient and usual to assume an ideal inverter, so that the desired voltages computed by the current control are applied to the machine. At low speed, the inverter nonlinear behavior, due to the dead-time introduced by the gate drive circuits and ON-state switch voltage drops, leads to an error between the command voltage vector and the real voltage vector applied to the machine.

For this reason, a feedforward dead-time compensation scheme has been implemented (Fig. 3). This scheme uses the reference currents that are transformed in phase quantities by means of a $(d,q) \rightarrow (abc)$ transformation (Fig. 3). The inverter phase duty-cycles (computed from the phase command voltages generated by the current control) are then modified by a compensation duty cycle according to

$$\delta'_\chi = \delta_\chi + \Delta\delta_\chi^{\mathrm{error}}, \qquad \chi = as, bs, cs \qquad (11)$$

where δ_χ is the phase duty cycle computed from the phase command voltage v_χ^*.

The compensation duty-cycle $\Delta\delta_\chi^{\mathrm{error}}$ (in per unit) is computed for each inverter phase as [13]

$$\Delta\delta_\chi^{\mathrm{error}} = \mathrm{sgn}\left(i_\chi^*\right) \cdot v_{\mathrm{error},abc},$$
$$\chi = as, bs, cs; \qquad v_{\mathrm{error},abc} = t_{\mathrm{d}} \cdot f_{\mathrm{SW}} \qquad (12)$$

where f_{SW} is the inverter switching frequency, t_{d} is the inverter dead time, and $\mathrm{sgn}(i_\chi^*)$ are the sign functions of the phase reference currents i_{abcs}^*.

In practice, this scheme can be used to also compensate the power switch threshold voltage v_{th} [2] that represents the main component of the power switch forward voltages. This compensation is performed by adjusting the voltage error
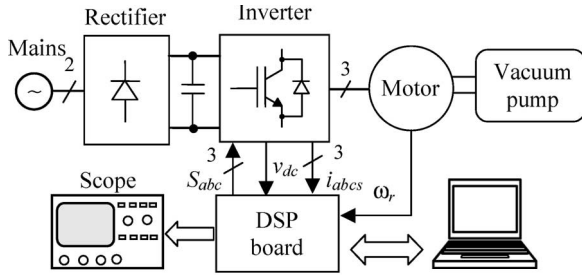
Fig. 4.   Experimental setup with vacuum pump.

$v_{\mathrm{error},abc}$ to get sinusoidal command voltages $v^*_{\mathrm{s}\alpha\beta}$ in stationary reference frame. The final inverter duty-cycle commands are used to obtain the inverter switching functions by means of the DSP digital pulsewidth modulation modulator.

IV. EXPERIMENTAL RESULTS

The experimental tests have been performed with a 0.5-kW three-phase induction motor driving a vacuum pump for industry applications (Fig. 4). An insulated gate bipolar transistor (IGBT) inverter whose switching frequency has been set at 8 kHz supplies the motor. The motor phase currents are measured by means of shunt resistances mounted between the emitters of bottom IGBTs and the negative dc-link rail. The motor speed is measured by means of an encoder only for comparison with the estimated speed.

The control algorithm has been implemented on a digital platform based on the 16-bit, fixed-point Motorola DSP56F803 controller. The control sampling frequency is 8 kHz. During execution of the control routine, the DSP can save data into its external memory; the data can be read and saved on a PC in Matlab format using the features of the DSP development software. In addition, up to 4 D/A channels on the board can be used to visualize in real-time the time variations of different variables.

The load torque given by the vacuum pump depends on speed and on the temperature of the lubrication oil. A strong ripple is superimposed on the average torque, resulting in a nonnull stall torque. The transient response to a speed step command between 0 and 1400 r/min (the pump works only for positive speeds) is shown in Fig. 5, while the drive response to a load step change (acting on the pump valve) is illustrated in Fig. 6. As shown by these tests, the drive response is good and fulfills the load requirements. The error between the real speed and estimated speed is small in this speed range (in Figs. 5 and 6 the real speed and the estimated speed waveforms practically overlap). It must be noted here that zero or very low speed operation is not required by the application, as well as a high accuracy of speed estimation.

To investigate the rotor flux observer performance, the measured currents and the observed currents are shown in Figs. 7 and 8 at pump startup. It should be noted how the observed currents converge very fast to the measured ones. To improve the observer performance at startup, the observed currents and rotor fluxes can be properly initialized during the machine fluxing period, as shown in Figs. 7 and 8. The observed rotor
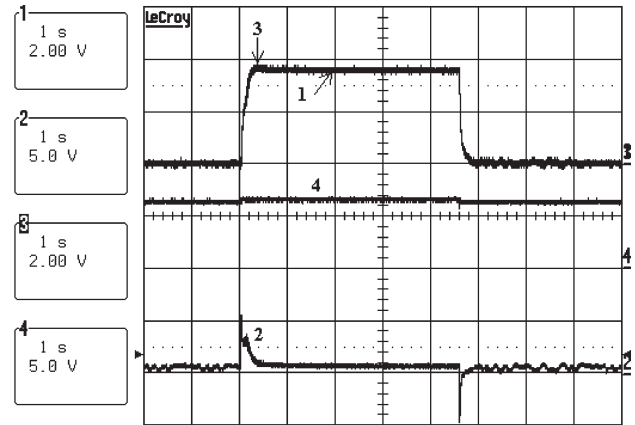

Fig. 5.   Drive response to speed step command $0 \div 0.36$ per unit (10 V/1 per unit). (1) $\hat{\omega}_{\mathrm{r}}$ (in per unit). (2) i_{qs} (in per unit). (3) ω_{r} (in per unit). (4) $\hat{\lambda}_{\mathrm{r}}$ (in per unit).
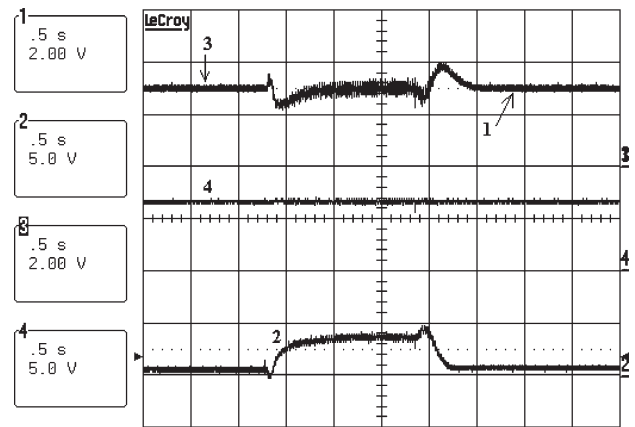

Fig. 6.   Drive response to load step change (10 V/1 per unit). (1) $\hat{\omega}_{\mathrm{r}}$ (in per unit). (2) i_{qs} (in per unit). (3) ω_{r} (in per unit). (4) $\hat{\lambda}_{\mathrm{r}}$ (in per unit).
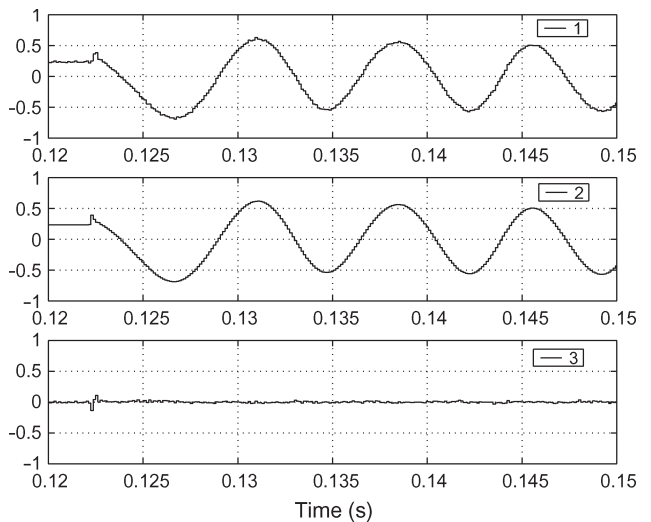

Fig. 7.   Measured and estimated α-axis currents at startup. (1) $i_{\mathrm{s}\alpha}$ (in per unit). (2) $\hat{i}_{\mathrm{s}\alpha}$ (in per unit). (3) $\varepsilon_\alpha = i_{\mathrm{s}\alpha} - \hat{i}_{\mathrm{s}\alpha}$ (in per unit).

flux components at startup (after the initial fluxing period) are shown in Fig. 9, demonstrating good transient response of the estimation scheme.
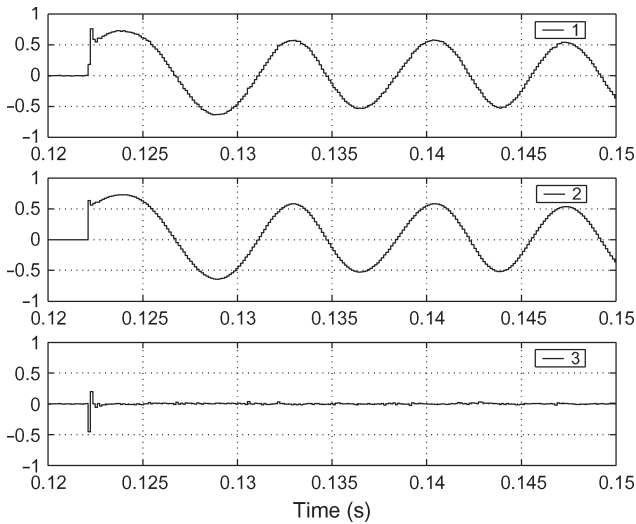
Fig. 8. Measured and estimated β-axis currents at startup. (1) $i_{s\beta}$ (in per unit). (2) $\hat{i}_{s\beta}$ (in per unit). (3) $\varepsilon_\beta = i_{s\beta} - \hat{i}_{s\beta}$ (in per unit).
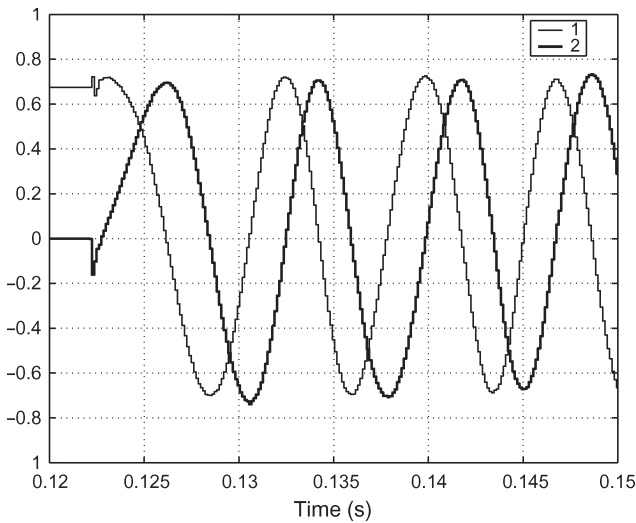

Fig. 9. Observed rotor flux components at startup. (1) $\hat{\lambda}_{r\alpha}$ (in per unit). (2) $\hat{\lambda}_{r\beta}$ (in per unit).
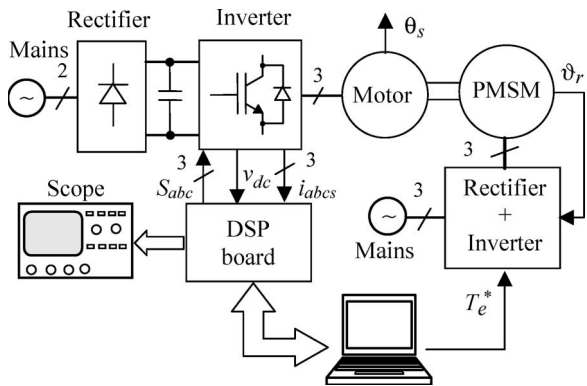

Fig. 10. Laboratory test rig.

As explained earlier, the vacuum pump requires only positive speed in a limited range. For this reason, the same motor type has been used in a laboratory test rig illustrated in Fig. 10.
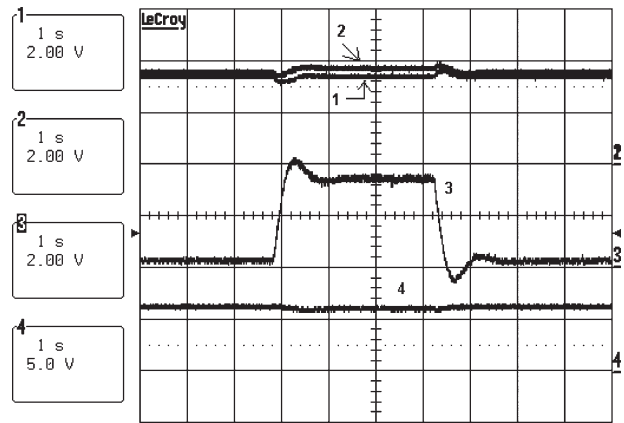

Fig. 11. Load rejection behavior at the limit of constant torque region (10 V/1 per unit). (1) $\hat{\omega}_r$ (in per unit). (2) $\hat{\omega}_e$ (in per unit). (3) i_{qs} (in per unit). (4) $\hat{\lambda}_r$ (in per unit).
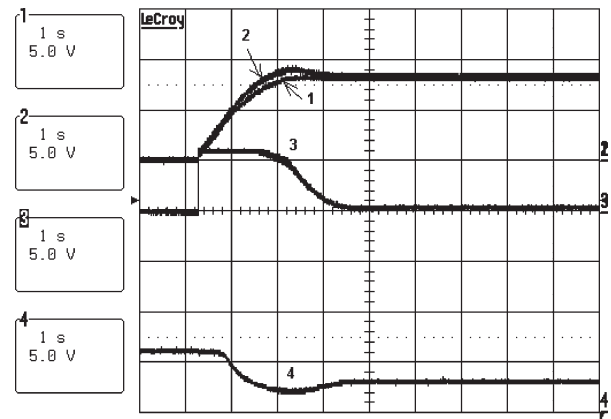

Fig. 12. Drive startup with inertial load up to 0.8 per unit (3100 r/min). (10 V/1 per unit). (1) $\hat{\omega}_r$ (in per unit). (2) $\hat{\omega}_e$ (in per unit). (3) i_{qs} (in per unit). (4) $\hat{\lambda}_r$ (in per unit).

The induction motor is loaded by means of a torque-controlled, permanent-magnet synchronous motor. The temperature θ_s of the induction motor stator end windings is monitored using a thermocouple.

The load rejection behavior of the drive for a speed of 0.35 per unit (limit of the constant torque region) is shown in Fig. 11 for a motor stator end windings temperature of about 85 °C. The applied load torque is about 120% of the motor rated torque. A good field orientation is noted since the rotor flux remains almost constant.

At the same stator end windings temperature, the drive transient performance involving field-weakening operation is shown in Fig. 12 for drive startup from standstill up to 0.8 per unit ($\cong$3100 r/min), while Fig. 13 illustrates the drive speed reversal from −0.8 to 0.8 per unit.

As an extreme operating condition, Fig. 14 shows the transient response of the drive for a short step load torque higher than the maximum motor torque. The SFOC shows robust orientation even in extreme situations (Fig. 14), and in general, good robustness against parameter detuning (stator and rotor resistance).

The drive performance is seriously altered at low speed, when the command voltages are highly distorted to impose
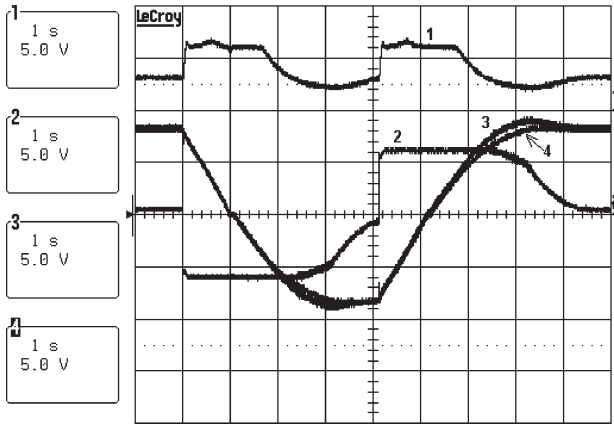
Fig. 13. Speed reversal from -0.8 to 0.8 per unit (10 V/1 per unit). (1) $\hat{\lambda}_r$ (in per unit). (2) i_{qs} (in per unit). (3) $\hat{\omega}_e$ (in per unit). (4) $\hat{\omega}_r$ (in per unit).
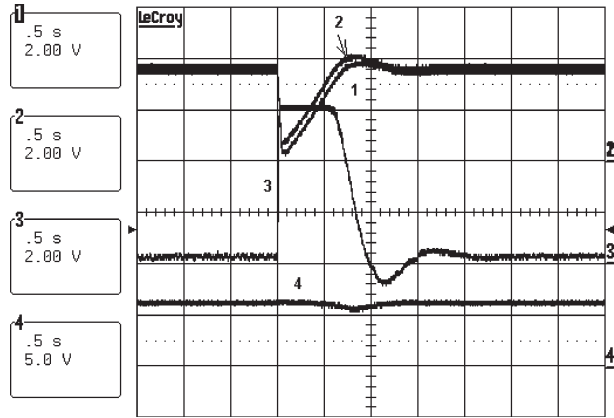

Fig. 14. Short step load change higher than the maximum motor torque. (10 V/1 per unit). (1) $\hat{\omega}_r$ (in per unit). (2) $\hat{\omega}_e$ (in per unit). (3) i_{qs} (in per unit). (4) $\hat{\lambda}_r$ (in per unit).
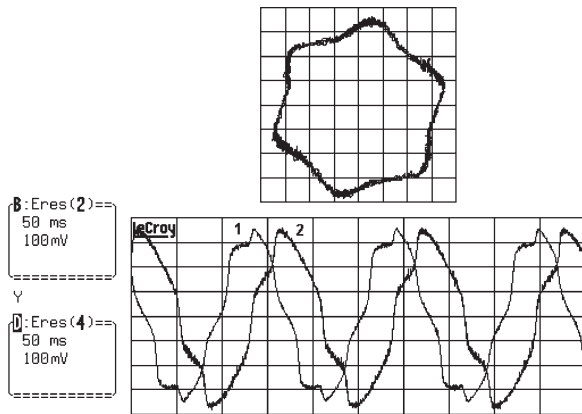

Fig. 15. Stator command voltage components and voltage vector locus in stationary reference frame at low speed (10 V/1 per unit) without dead-time compensation. (1) $v^*_{s\alpha}$ (in per unit). (2) $v^*_{s\beta}$ (in per unit).

sinusoidal currents (Fig. 15). When enabled, the dead-time compensation scheme (Fig. 3) eliminates the command voltages distortion, as shown in Fig. 16.

At zero speed the field orientation is robust only at light loads. For higher loads, the behavior at zero speed is dominated by the stator resistance detuning. For this reason, the proposed
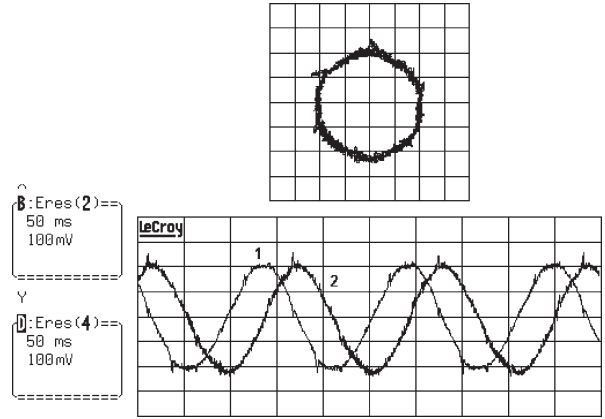

Fig. 16. Stator command voltage components and voltage vector locus in stationary reference frame at low speed (10 V/1 per unit) with dead-time compensation. (1) $v^*_{s\alpha}$ (in per unit). (2) $v^*_{s\beta}$ (in per unit).

SRDFOC scheme is suitable for applications not requiring very low speed operation.

For applications requiring high speed estimation accuracy and/or operation at very low speed, particular stator resistance estimation schemes must be used [2].

V. CONCLUSION

This paper deals with an SDRFOC scheme for three-phase induction motor drives to be employed in low-cost applications. A sensorless closed-loop rotor flux observer was used for rotor flux estimation. The observer is very simple to implement with low-cost fixed point DSP controllers, making it an attractive solution to replace the traditional V/Hz open-loop control. The effectiveness of the observer is demonstrated by experimental results obtained for a low cost vacuum pump drive and a laboratory test rig.

APPENDIX

The prototype is a 0.5-kW 135 V/50 Hz 4.6 A four-pole, three-phase induction machine with the following parameters: $R_s = 2.175~\Omega$, $R_r = 1.9~\Omega$, $L_{ls} = L_{lr} = 4.68$ mH, $L_m = 86.6$ mH. The base quantities used for machine model normalization are: base voltage $V_{base} = 450$ V, base current $I_{base} = 15$ A and base electrical speed $\omega_{base} = 2 \cdot \pi \cdot 128$ rad/s. The complex gain of the observer is $\bar{g} = 0.5 + j0.1$ (in per unit).

REFERENCES

[1] H. Xu, Z. Zhang, and L. Heilman, "Sensorless direct field oriented control of three-phase induction motors based on 'sliding mode' for washing machine drive applications," in *Conf. Rec. IEEE IAS Annu. Meeting*, 2005, vol. 1, pp. 77–83.

[2] J. Holtz, "Sensorless control of induction motor drives," *Proc. IEEE*, vol. 90, no. 8, pp. 1359–1394, Aug. 2002.

[3] C. Schauder, "Adaptive speed identification for vector control of induction motors without rotational transducers," *IEEE Trans. Ind. Appl.*, vol. 28, no. 5, pp. 1054–1061, Sep./Oct. 1992.

[4] H. Kubota, K. Matsuse, and T. Nakano, "DSP-based speed adaptive flux observer of induction motor," *IEEE Trans. Ind. Appl.*, vol. 29, no. 2, pp. 344–348, Mar./Apr. 1993.

[5] Y.-R. Kim, S.-K. Sul, and M.-H. Park, "Speed sensorless vector control of induction motor using extended Kalman filter," *IEEE Trans. Ind. Appl.*, vol. 30, no. 5, pp. 1225–1233, Sep./Oct. 1994.

[6] V. I. Utkin, "Sliding mode control design principles and applications to electric drives," *IEEE Trans. Ind. Electron.*, vol. 40, no. 1, pp. 23–36, Feb. 1993.

[7] J. Li, L. Xu, and Z. Zhang, "An adaptive sliding-mode observer for induction motor sensorless speed control," *IEEE Trans. Ind. Appl.*, vol. 41, no. 4, pp. 1039–1046, Jul./Aug. 2005.

[8] A. Derdiyok, M. K. Guven, H. Rehman, N. Inanc, and L. Xu, "Design and implementation of a new sliding-mode observer for speed-sensorless control of induction machine," *IEEE Trans. Ind. Electron.*, vol. 49, no. 5, pp. 1177–1182, Oct. 2002.

[9] M. Tursini, R. Petrella, and F. Paralisiti, "Adaptive sliding-mode observer for speed-sensorless control of induction motors," *IEEE Trans. Ind. Appl.*, vol. 36, no. 5, pp. 1380–1387, Sep./Oct. 2000.

[10] C. Lascu, I. Boldea, and F. Blaabjerg, "Direct torque control of sensorless induction motor drives: A sliding-mode approach," *IEEE Trans. Ind. Appl.*, vol. 40, no. 2, pp. 582–590, Mar./Apr. 2004.

[11] K. Hurst, T. Habetler, G. Griva, and F. Profumo, "Zero-speed tacholess IM torque control: Simply a matter of stator voltage integration," *IEEE Trans. Ind. Appl.*, vol. 34, no. 4, pp. 790–795, Jul./Aug. 1998.

[12] A. Fratta, A. Vagati, and F. Villata, "Vector control of induction motors without shaft transducers," in *Proc. IEEE PESC*, 1988, vol. 2, pp. 839–846.

[13] J. K. Pedersen, F. Blaabjerg, J. W. Jensen, and P. Thogersen, "An ideal PWM-VSI inverter with feedforward and feedback compensation," in *Proc. EPE*, 1993, pp. 501–507.

Paolo Guglielmi (M'07) was born in Imperia, Italy, in 1970. He received the M.Sc. degree in electronic engineering and the Ph.D. degree in electrical engineering from the Politecnico di Torino, Turin, Italy, in 1996 and 2001, respectively.

In 1997, he joined the Dipartimento di Ingegneria Elettrica, Politecnico di Torino, where he became a Researcher in 2002. He has authored several papers published in technical journals and conference proceedings. His fields of interest include power electronics, high-performance servodrives, and computer-aided design of electrical machines.

Dr. Guglielmi is a Registered Professional Engineer in Italy.

Radu Bojoi (M'06) received the M.Sc. degree in electrical engineering from the "Gh. Asachi" Technical University of Iasi, Iasi, Romania, in 1993, and the Ph.D. degree from the Politecnico di Torino, Turin, Italy, in 2003.

From 1994 to 1999, he was an Assistant Professor with the Department of Electrical Utilization, Electrical Drives and Industrial Automation, "Gh. Asachi" Technical University of Iasi. In 2004, he joined the Dipartimento di Ingegneria Elettrica, Politecnico di Torino, as an Assistant Professor. He has published more than 20 papers in technical journals and conference proceedings. His main research field is DSP- and field-programmable-gate-array-based digital advanced control solutions for three-phase and multiphase electrical drives and power electronic converters.

Dr. Bojoi received the IPEC2005 Conference First Prize Award in 2005.

Gian-Mario Pellegrino (M'06) received the M.Sc. and Ph.D. degrees in electrical engineering from the Politecnico di Torino, Turin, Italy, in 1998 and 2002, respectively.

In 2002, he joined the Dipartimento di Ingegneria Elettrica, Politecnico di Torino, as a Research Associate, teaching power electronics and industrial electronics courses and supervising Ph.D. students. Deeply involved in research projects both for the public sector and for industry (FIAT, LG Electronics, and many local companies), he has more than 20 technical papers and two patents as a co-inventor. His areas of interest are synchronous and asynchronous ac drives, namely, in the motor design and digital control. He has worked in the fields of hybrid traction for cars and of design of direct-drive generators for wind energy production. He was a Guest Researcher with Aalborg University, Denmark, in 2002.